



ORIGINAL RESEARCH ARTICLE

Microstructure and Wear Performance of Fly Ash-Reinforced Copper Matrix Composites Prepared via Powder Metallurgy

Isaac Dinaharan , Thangadurai Albert, and Jebaraj David Raja Selvam

Submitted: 17 February 2023 / Revised: 22 August 2023 / Accepted: 20 September 2023

This research work investigated the role of fly ash particles (0, 5, 10, 15 and 20 wt.%) on the microstructural evolution and the wear resistance under dry sliding conditions of copper matrix composites (CMCs), prepared through powder metallurgy (PM) route. Copper and fly ash particles were initially mixed in a twin-shell blender, compacted in a die and sintered in a protected muffle furnace. Proper dispersion of fly ash particles was obtained. XRD plots did not show the formation of any other compounds or oxides. The increase in fly ash content increased porosity content. EBSD images of the composites revealed grain refinement due to the incorporation of fly ash particles. Fly ash reinforcement particles enhanced the resistance to wear and lowered the values of the coefficient of friction (COF). The wear mechanism shifted to abrasive wear from microcutting at particle content exceeding 10 wt.%. The electrical conductivity of the prepared CMCs was negatively affected by fly ash particles.

Keywords copper matrix composites, fly ash, microstructure, powder metallurgy, wear

1. Introduction

Copper conducts electricity and heat much faster compared to most of the metallic materials. It is largely used to manufacture electrical appliances as well as components requiring heat dissipation. Several components, such as nozzles and contact breakers, are subjected to sliding wear, arcing and particle impingement. Pure copper is easily worn and eroded. Thus, copper matrix composites (CMCs) were developed to protect the copper from accelerated wear and premature failure. Ceramic particles were often mixed with pure copper to prepare CMCs (Ref 1-4).

The density of pure copper is much higher than commonly reinforced ceramic particles. Producing CMCs by casting route is tedious due to the huge density difference, which prevents the particles from staying in suspension within the molten copper for a longer duration. Particles tend to float over the melt. The surface of the ceramic particles is poorly wetted by molten copper, leading to poor interfacial bonding and particle rejection. The higher casting temperature promoted unwanted chemical reactions with copper in addition to causing thermo-

dynamic instability of the reinforcement to stay without disintegration (Ref 5-8). Melting of copper is to be stopped during processing to eliminate these setbacks. Friction stir processing (FSP) was preferred for making CMCs for the past several years (Ref 9). FSP effectively overcomes the limitations of the casting route. Nevertheless, FSP has its own limitations, such as optimization of a large number of process parameters, undue tool wear, improper distribution of particles over the stir zone, particle fracture and low volume fraction (Ref 10-12). Powder metallurgy (PM) route still remains as a good processing method for preparing CMCs and offers excellent control over the microstructure evolution (Ref 13). Proper distribution of particles can be obtained effortlessly compared to FSP (Ref 14).

Ceramic particles such as SiC (Ref 15), Al₂O₃ (Ref 16), TiC (Ref 17), B₄C (Ref 18) and TiB₂ (Ref 19) were widely used to reinforce CMCs. Ceramic particles usually increase the production cost. Fly ash is considered as economical and potential reinforcement for metallic composites which have aluminum, magnesium and copper as matrix material (Ref 20). The typical composition of fly ash consists of silicon oxide (SiO₂), alumina (Al₂O₃) and calcium oxide (CaO) predominantly. Fly ash is a by-product of the combustion of coals in thermal plants around our planet Earth. The flue gas of the combustion is filtered before letting into the atmosphere to capture fly ash particles. Every day, tons of fly ash are released, which poses a threat to pollute the fertile land. Solid and hollow types of fly ash particles are available (Ref 21-24).

The PM route was explored to manufacture fly ash-reinforced CMCs. Sai et al. (Ref 25) reinforced copper-coated fly ash particles (0-16 wt.%) into Cu-5%Sn to prepare CMCs. They concluded that the copper coating improved the density and other mechanical properties. Chew et al. (Ref 26) developed Cu/30 wt.% fly ash and studied the effect of sintering temperature. Increased sintering temperature caused a reduction in density. The samples began to melt beyond a

Isaac Dinaharan, Department of Mechanical Engineering Science, University of Johannesburg, Auckland Park Kingsway Campus, Johannesburg 2006 Gauteng, South Africa; **Thangadurai Albert**, Department of Mechanical Engineering, V V College of Engineering, Tisaiyanvilai, Tamil Nadu 627657, India; and **Jebaraj David Raja Selvam**, Department of Mechanical Engineering, Karunya Institute of Technology and Sciences, Coimbatore, Tamil Nadu 641114, India. Contact e-mail: dinaweld2009@gmail.com.

sintering temperature of 1000 °C. Balamurugan and Uthayakumar (Ref 27) prepared Cu/(5-10 wt.%) fly ash CMCs and investigated the role of processing conditions. An increase in compaction pressure, sintering temperature and sintering time improved the density and the mechanical properties of the composite. Kasirajan et al. (Ref 28) fabricated Cu/(3-12 wt.%) fly ash CMCs and observed a drop in the electrical and the thermal conductivity of the composite. Fly ash particles were advantageous for reducing the specific wear rate. Balamurugan et al. (Ref 29) produced Cu/(2.5-10 wt.%) fly ash CMCs and investigated the sliding wear under dry conditions. The increased content of fly ash was helpful in improving wear resistance. Increased load and velocity induced a change in the wear mechanism from plastic deformation to delamination. Devaraju et al. (Ref 30) attempted to prepare Cu/(5 wt.% SiC + 5 wt.% fly ash) hybrid CMC and noticed a decrease in wear rate due to fly ash reinforcement. Rajesh et al. (Ref 31) prepared Cu/(3-9 wt.%) fly ash CMCs and applied conventional and microwave sintering. They found that microwave sintering improved the properties to some extent.

The interest in utilizing fly ash as reinforcement for CMCs is constantly growing. Limited literature is available on this topic. More works are required to establish this composite material. This study encompasses the production of Cu/(0-20 wt.%) fly ash CMCs using the PM method and carries out the advanced characterization of the microstructural features such as EBSD and wear performance under dry sliding conditions. The role of fly ash particle and its content is presented in detail. The volume content is also relatively high compared to existing works.

2. Experimental Procedure

Pure copper and fly ash powders were used as starting materials for producing CMCs. Figure 1 presents the SEM micrographs of copper and fly ash powders. Pure copper powder was supplied by M/s Alfa Aesar. It exhibits flake morphology (Fig. 1a). Fly ash powders were collected from a Thermal Power Station located at Tuticorin, India. The morphology of fly ash particles is spherical (Fig. 1b), and it is classified as solid precipitator kind of fly ash. The particle size distribution was analyzed using MALVERN Mastersizer 2000. The particle size distribution is shown in Fig. 2. The

average particle size of copper and fly ash was, respectively, 21 μm and 6 μm . Table 1 shows the composition of collected fly ash particles. The composition was estimated by x-ray fluorescence (XRF). A twin shell, which was attached to a revolving lathe chuck, was used for blending copper and fly ash powders. The twin shell was rotated for 2 h at 300 rpm. Balls made of stainless steels, having a diameter of 10 mm each, were introduced into the twin shell. The ratio of ball to powder charge was fixed as 10. The balls were introduced in order to promote cold welding between pure copper and fly ash powders. Powders were blended at different weight percentage of fly of particles (0 wt.%, 5 wt.%, 10 wt.%, 15 wt.% and 20 wt.%). PM method is applied to reinforce medium to a high volume of reinforcement particles into the copper matrix. A maximum content of 20 wt.% is considered to be a reasonable choice based on the published literature on CMCs. The blended powders were transferred into a die that was fabricated for the compaction process. The internal diameter of the die was 20 mm. The die was placed on a universal tensile testing machine having a capacity of 3000 kN. A compressive force of 250 kN was gradually applied to compact the blended powders. The green compacts were subsequently transferred to a muffle furnace for sintering. The temperature of the furnace was maintained at 950 °C. Each sample was held at this temperature for 2 h. The furnace was provided with an inert atmosphere and protection to avoid oxidation. The parameter in each step was carefully chosen based on several trial experiments to obtain samples having good strength without fragility. The procedure to make CMCs was presented in an earlier research work (Ref 32).

Five-millimeter-thick circular samples were sliced for metallographic observation. Each sample was meticulously grounded and polished using a semi-automatic polishing machine. Both alumina and diamond suspension was used in the final polishing stage to obtain a flat surface resembling a mirror finish. A chemical reagent comprising 15 HCl, 2.5 g FeCl_3 in 100 mL H_2O was prepared to intentionally corrode the polished surface to reveal the microstructure. Etched samples were observed using an optical microscope (OLYMPUS BX51 M) and a field emission electron microscope (CARL ZEISS-SIGMAHV). EBSD observation was accomplished in a FEI Quanta FEG SEM supplied with TSL-OIM software. X-ray diffraction patterns (XRD) of the samples were recorded using Shimadzu XRD 6000. Theoretical density and experimental density were, respectively, estimated by the rule of the mixture

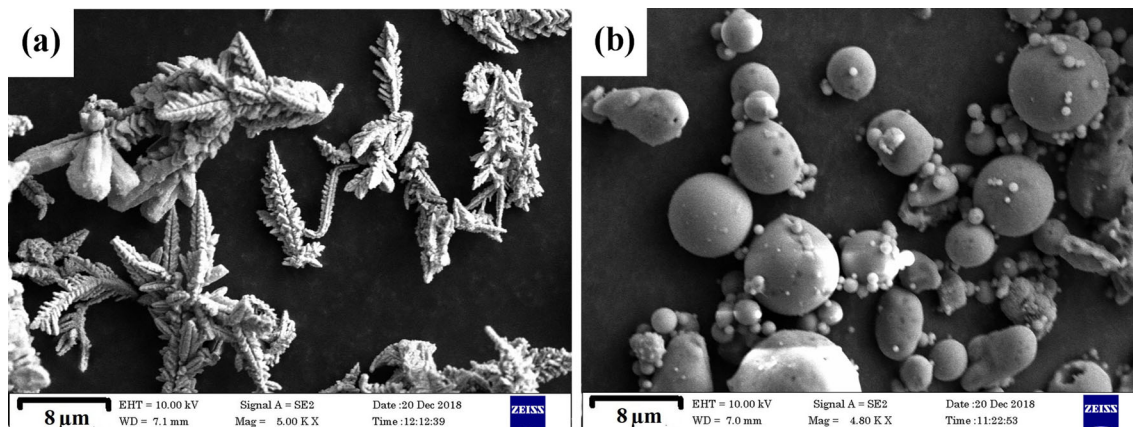


Fig. 1 SEM micrographs of: (a) copper particles and (b) fly ash particles

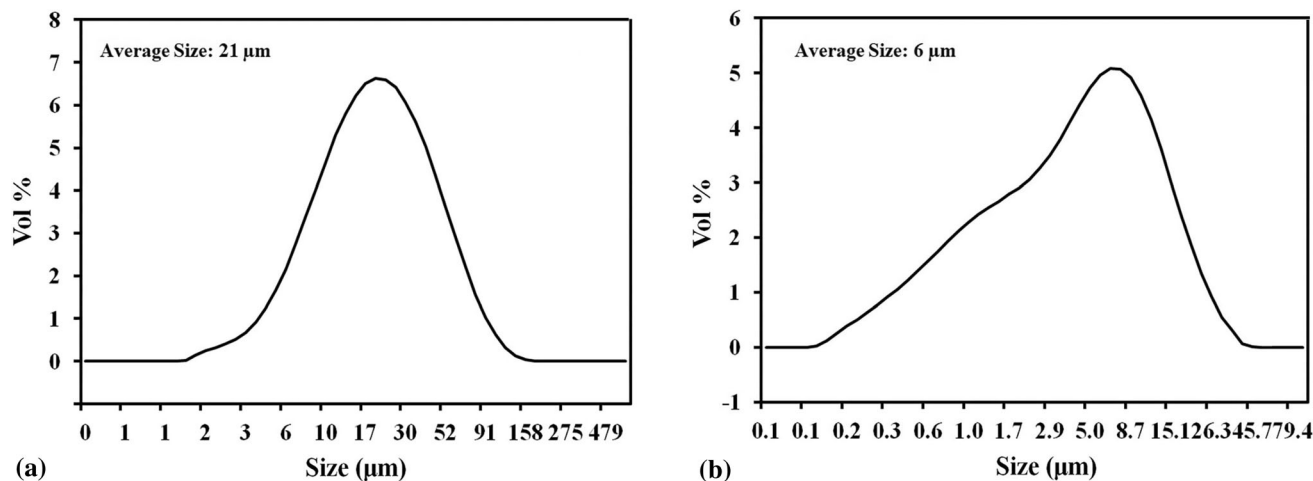


Fig. 2 Particle size distribution of: (a) copper particles and (b) fly ash particles

Table 1 Chemical composition of fly ash

Element	SiO ₂	Al ₂ O ₃	Fe ₂ O ₃	CaO	MnO ₂	K ₂ O	TiO ₂	Na ₂ O	LOI*
wt.%	49.50	25.54	8.92	6.13	1.03	0.65	0.53	0.47	Balance
LOI loss on ignition									

and Archimedes principle. The density of the collected fly ash particles was 2300 kg/m³. Percentage porosity was subsequently calculated based on the difference in theoretical density and experimental density. Four-point probe method was used to estimate the electrical conductivity. The four-point probe tester had a dynamic nitrogen atmosphere with varying temperature. The electrical contacts were made using pure indium metal. Platinum wires of 0.5 mm diameter were used for connection. Direct current was used for recording the measurements. The junction points were polished for improving the contact. A thin layer of silver paste having high conductivity was applied to prepare the contact points via adhesion. A thermocouple was used for varying the temperature.

The sliding wear behavior of the composite specimens without adding any lubricant was evaluated using pin-on-disc-type computerized wear equipment (DUCOM TR20-LE) according to ASTM G99 standard. Specimens having a square cross section (5 mm × 5 mm) were machined out from the sintered samples. The samples were slid on a hardened chromium steel counter disc at a speed of 1.5 m/s to a distance of 2000 m. A load of 20 N was applied on the specimens. The parameters were chosen based on the maximum limit of the wear test apparatus so that the height loss will not exceed the limit of 2000 μm but give variation to compare between samples. The specimen eventually lost its height as a result of sliding. The reduction in the height of the specimen was recorded in the software associated with the wear tester. The reduction in height was translated into wear rate. The worn surface of each sample, along with the fallen debris, was observed using a scanning electron microscope. The worn surfaces of selected samples were further observed using a profilometer (Veeco Nt-1100) to record 3D morphology and surface roughness.

3. Results and Discussion

3.1 Microstructure of Blended Powders

Figure 3 presents the morphology of the blended and milled powders of copper and fly ash having 10 and 20 wt.%. The SEM micrographs show that copper and fly ash particles are blended well. There is no severe agglomeration of fly ash particles which is well dispersed. The blending time is sufficient to achieve a reasonable mixture of composite powders. Further, the added steel balls cause an effect of mechanical milling to some extent. There are few changes in the morphology of powders. Mechanical milling usually causes fracture of hard reinforcement particles, flattening of the ductile matrix and subsequent cold welding and fracture (Ref 33). Several fly ash particles retain the original spherical shape. The retention of shape is due to two causes; (a) spherical-shaped particles have a tendency to slip through the steel balls easily (Ref 34) and (b) the blending duration was only a few hours in contrast to long milling hours, which may be insufficient to knock down the particle for altering its shape and size. Nevertheless, there is evidence of cold welding and fracture in Fig. 3. Agglomerates of cold-welded copper particles and embedded fly ash particles are visible. The energy of ball collision is transferred to the copper particle, which in response flattens and forms a lamellar structure. The flattened copper particles are subsequently cold welded and fracture again. The fly ash particles are trapped between the interfaces of cold-welded copper particles, which are marked in Fig. 3.

3.2 XRD of Cu/Fly Ash CMCs

X-ray diffraction patterns pertaining to the sintered composites are plotted in Fig. 4. The plot presents the peaks of

copper and the composition ingredients of fly ash such as SiO_2 , Al_2O_3 and Fe_2O_3 . SiO_2 peaks are well pronounced compared to other elements of the fly ash particle because of the high percentage in the composition, according to Table 1. SiO_2 peaks become taller at a higher volume fraction of 20 wt.%. The increased content of the reinforcement particle usually

increases the peak height because of increased particle count, and the presence of more crystal planes increases the probability of detection. Peaks of any other oxides or interfacial reaction products were not detected. There is no palpable shift in the peaks of copper and fly ash, indicating the absence of any other compound. The sintering temperature, sintering duration

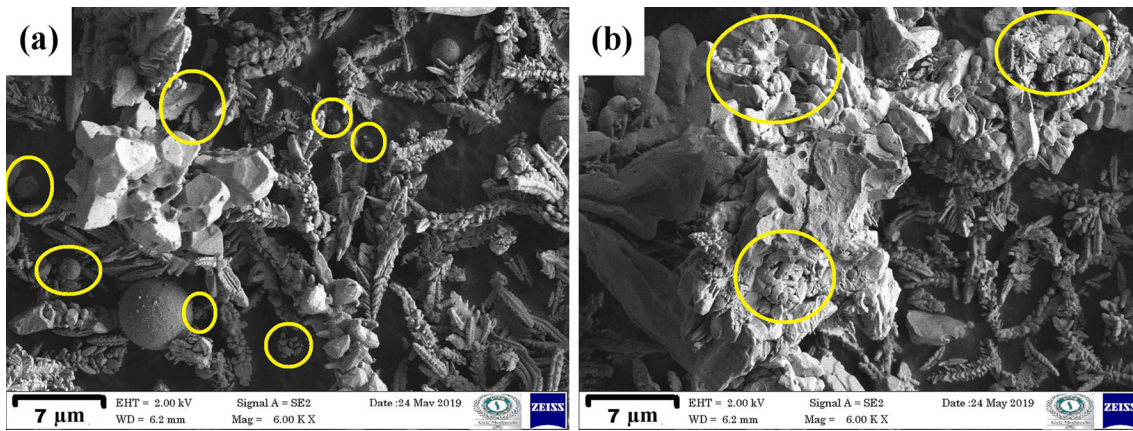


Fig. 3 SEM micrographs of blended and milled particles having fly ash content: (a) 10 wt.% (fractured fly ash particles are circled) and (b) 20 wt.% (cold welding spots are circled)

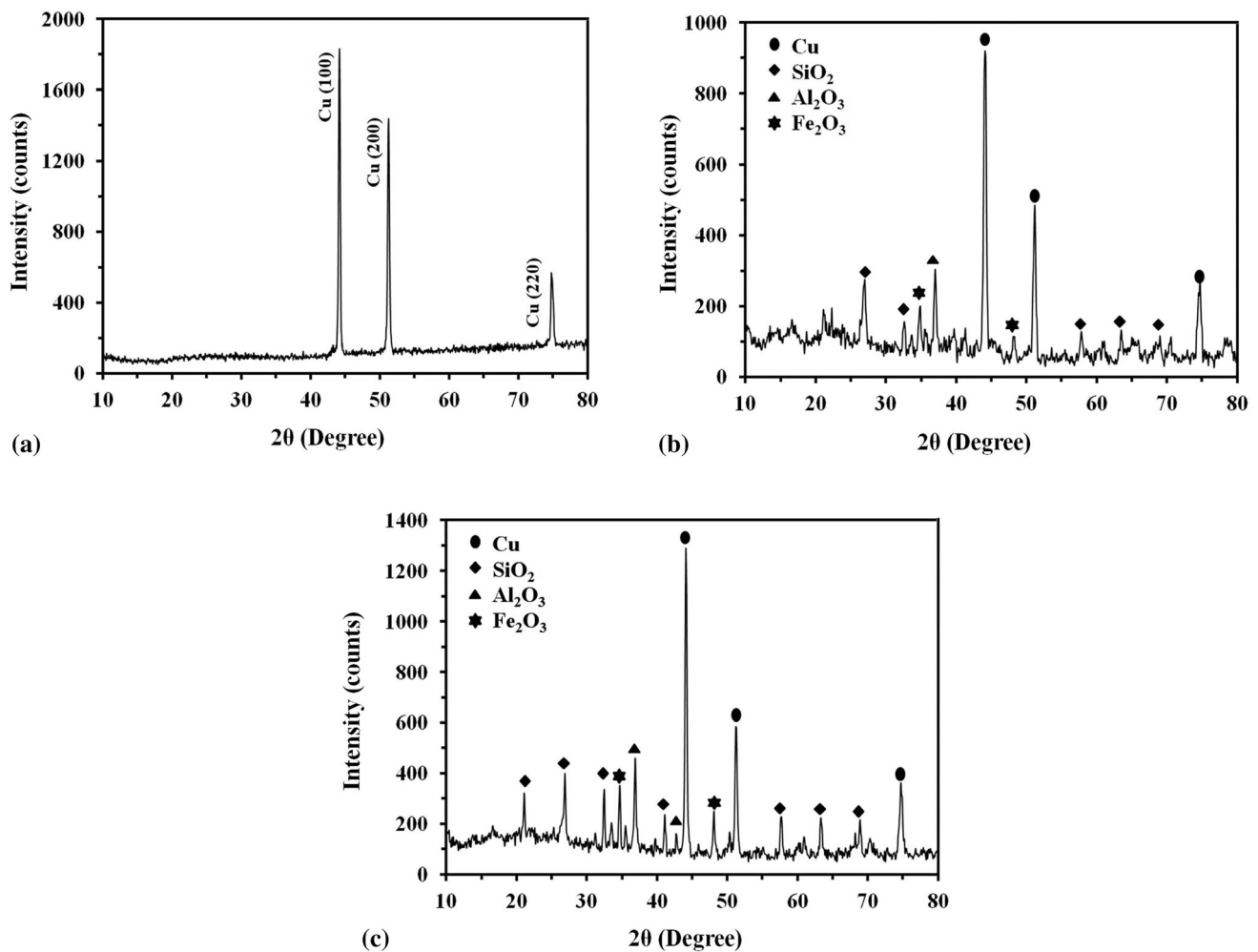


Fig. 4 XRD patterns of Cu/fly ash CMCs containing fly ash particles: (a) 0 wt.%, (b) 10 wt.%, and (c) 20 wt.%

and atmosphere of the sintering furnace play a role in oxidation and initiating unsolicited chemical reactions. Copper tends to react with O_2 and produces Cu_2O during sintering (Ref 18). Since the furnace was provided with highly purified argon gas, the copper oxidation was suppressed. The temperature during sintering stage is critical to influence the oxidation behavior of copper, as concluded by earlier investigators (Ref 35). They observed the excessive formation of Cu_2O , when the sintering furnace temperature was maintained at 950 °C. Although the present work employed the same sintering temperature, there is no significant formation of Cu_2O to be detectable by the XRD. This can be correlated to the type of furnace used for sintering. They used an open atmospheric furnace in contrast to the closed furnace used in this investigation. The former is more prone to oxidation than the latter.

3.3 Microstructure of Cu/Fly Ash Composites

SEM micrographs of the prepared Cu/fly ash CMCs are shown in Fig. 5. Particles are spread across the micrographs. The number of fly particles increases with an increase in reinforcement content. No region is left without any distribution of particles. Since sintering does not melt the copper matrix, issues such as segregation at grain boundary regions are totally absent. Therefore, the nature of the distribution can be considered to be homogeneous. Nevertheless, few clusters are spotted at higher particle content (Fig. 5d). A proper distribution of reinforcement is a basic requirement in a metallic composite system for the enhancement of mechanical and

sliding wear performance because the nature of distribution is a dominating factor compared to all other microstructural features (Ref 36). SEM micrographs (Fig. 5) reveal that there is no particle dropout during the metallographic preparation of the samples. This could possibly hint a proper adherence and good bonding of fly ash particles with the copper matrix. The copper matrix in the composite is seen as continuous without any other defects, such as large-size pores or voids. This observation assures proper consolidation of copper and fly ash particles during compaction and sintering. As seen in Fig. 5, which showcases the SEM micrographs, many fly particles exhibit the initial spherical morphology without a change. The mechanical damage and chemical disintegration during composite preparation are negligible. Spherical-shaped reinforcement particles are beneficial to evade needless stress build up during the application of tensile or normal loading.

Figure 6 plots the relative density and porosity for different content of fly ash particles. The relative density is less than 100% for the composites. This indicates that the density of the sintered composites (Fig. 6a) is lower than that of the theoretical density. The porosity content increases with the increase in the fly ash content (Fig. 6b). Particles are rearranged during the process of compaction. Some particles are plastically deformed to cause a movement. The compaction pressure was kept constant for all specimens. Consequently, the densification by the movement of plastically deformed particles is almost identical. Thus, the density variation is due to fly ash density in addition to its influence while sintered. The fly ash density is

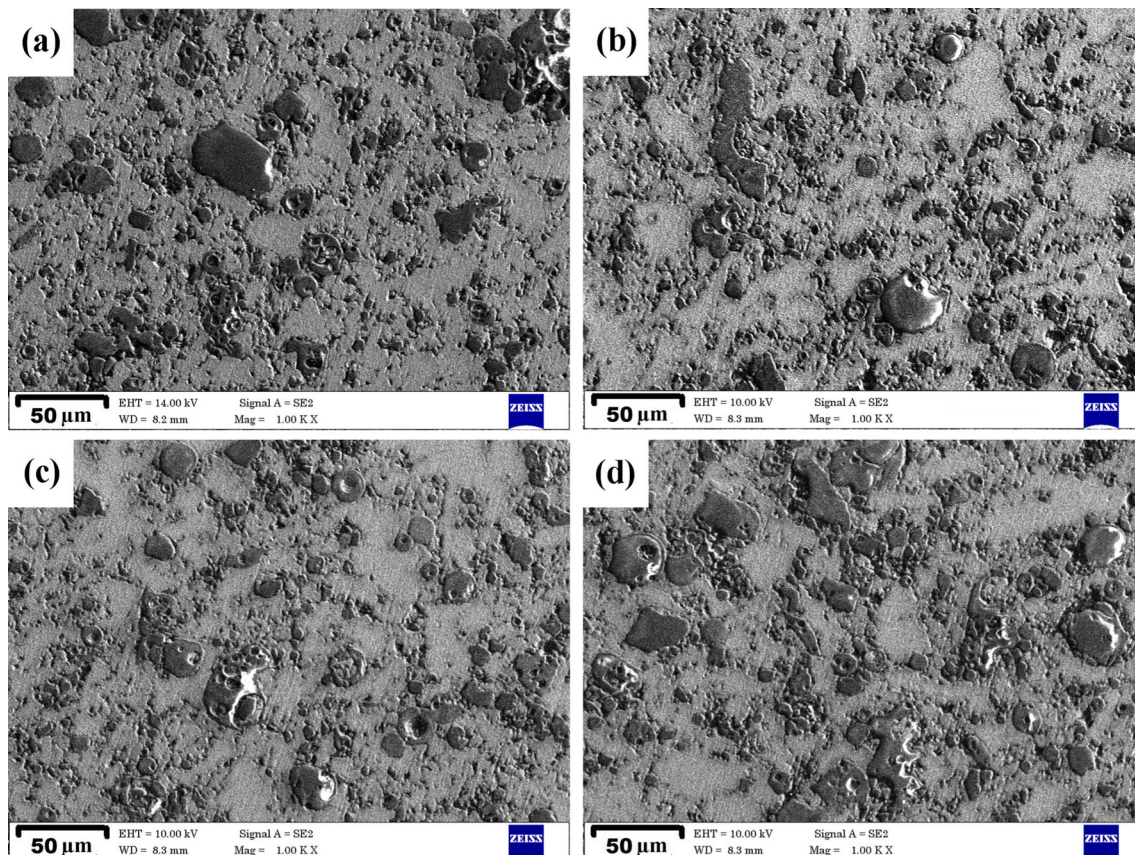


Fig. 5 SEM micrographs of Cu/fly ash CMCs containing fly ash particles: (a) 5 wt.%, (b) 10 wt.%, (c) 15 wt.%, and (d) 20 wt.%

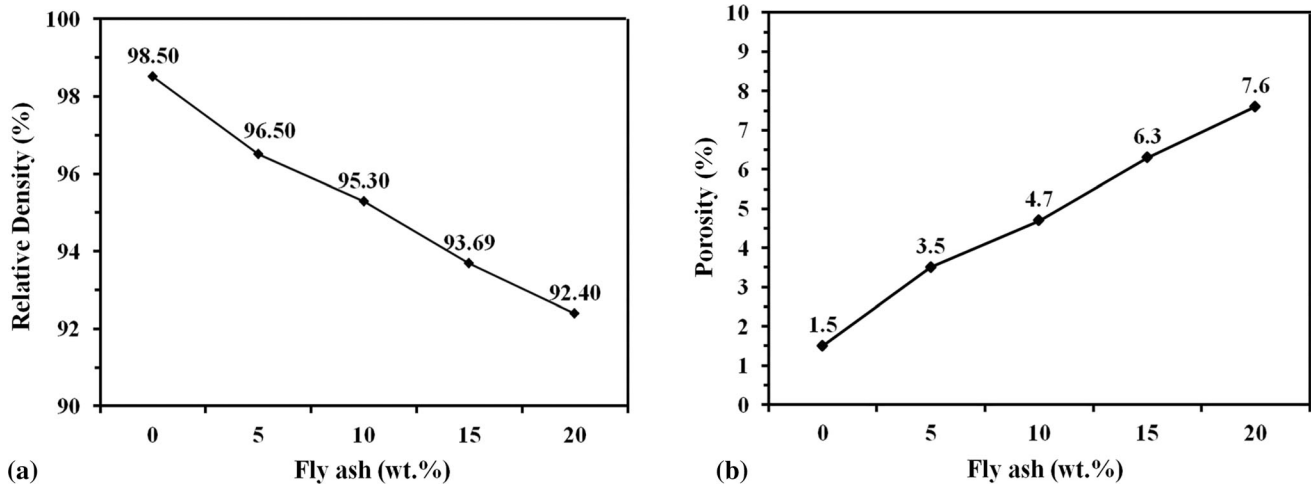


Fig. 6 (a) Relative density and (b) porosity of prepared Cu/fly ash CMCs

almost four times lighter than the copper matrix. Adding a reinforcement having lower density would obviously lower the resultant composite density. This is beneficial for boosting the specific strength of the composite. Secondly, the fly ash particle is present as an obstacle during the sintering process. Metallic bonds are created during sintering, and most of the pores are eventually closed. The copper fly ash interface acts as a barrier to the diffusion mechanism. This is commonly observed in sintered metallic composites reinforcement with ceramic particles (Ref 37). This leads to a lowering of density as well as an increase in porosity content. The higher porosity content at higher content of fly particles is attributed to the tendency to form clusters. Few clusters are present at high fly ash contents additionally inhibit diffusion and cause lower density in addition to pore formation. The melting point of fly ash particles is roughly 400 °C higher than the selected sintering temperature. Therefore, direct contact between particles in a cluster affects sintering (Ref 25). Further, the number of copper fly ash interfaces at higher weight percentage is relatively high. The efficiency of the diffusion of copper particles is reduced to another level.

Figure 7 shows a representative SEM micrograph of Cu/15 wt.% fly ash CMC (Fig. 9a) and mapping of elements present in the composite such as Cu (Fig. 7b), Si (Fig. 7c), Al (Fig. 7d), and Fe (Fig. 7e). The elements are mapped in different colors. The matrix occupies the major portion of the micrograph in a continuous manner. Elemental mapping confirms the observation made using SEM micrographs in Fig. 5. The homogenous dispersion of elements in the copper matrix ensures that the fly ash particles are distributed properly without severe clustering. Most of the fly ash particles are separated by an interparticle distance. Elemental mapping does not show the existence of pores in significant quantity. Further, localized regions consisting of enriched elements are not found. This result hints at the absence of undesirable chemical reactions in larger quantities.

Figure 8 shows an enlarged view of a single particle in Cu/20 wt.% fly ash CMC (Fig. 8a) and a line EDAX across this particle (Fig. 8b). The amount of each element varies sharply at the interface without any gradual change. This indicates that the chemical interaction between copper and fly ash is absent or negligible. No other compounds or reaction products are formed during processing. The SEM image of the interface in Fig. 8a confirms this observation. The interfacial boundary at

the edge of the fly ash particle is clearly delineated. The interfacial boundary is not interrupted by foreign compounds or chemical products or pores. These interfacial features are desirable for obtaining a strong interfacial bonding in a metallic composite system because the applied external load would be effectively transferred to the particle. The copper matrix encloses the fly ash particle, indicating proper compaction as well as sintering conditions. There are two kinds of bonding that take place between a metallic matrix and a ceramic reinforcement particle in composites processed by the PM route. The reinforcement particles are interlocked mechanically with the metallic matrix. A chemical bond is established via diffusion in a solid state (Ref 38). Sintering promotes a solid-state diffusion between fly ash particles and copper without adverse reactions to form a chemical bond. The element count of Cu is not zero at the interface crossing. This indicates a chemical bond and diffusion of copper atoms.

Figure 9 shows the EBSD images belonging to the fabricated Cu/fly ash CMCs. The grain structure of the composite and the role of fly ash particles are visualized. EBSD images were not subjected to cleaning procedure to remove the locations, where fly particles were reinforced. The number, marked at the top right corner in each image, is the average grain size. It is understood that the increase in fly ash particle content leads to a reduction in grain structure. The possible sintering mechanism responsible for the consolidation of the compacted powders is diffusion. Sintering mechanisms, which occur in liquid state and vapor state, do not occur, due to the set sintering temperature and the composition of the composite powders. In case of sintering pure copper, local bonding occurs at the contact point between particles. As time lapses, it grows into necking, and finally, a grain boundary is formed. The grain would grow in size depending on the sintering temperature and duration (Ref 34). In case of sintering composite powders, the fly ash reinforcement particles hinder the direct diffusion between copper powders. The area of hindrance depends on the number of fly ash particles and their weight fraction. The presence of fly ash particles restricts the further growth of copper grains after diffusion occurs. The resistance to grain growth increases at higher content of fly ash particles. Since a constant sintering time was kept for all samples, the increased fly ash content decreases the time available for grain growth. Therefore, the grain size decreases

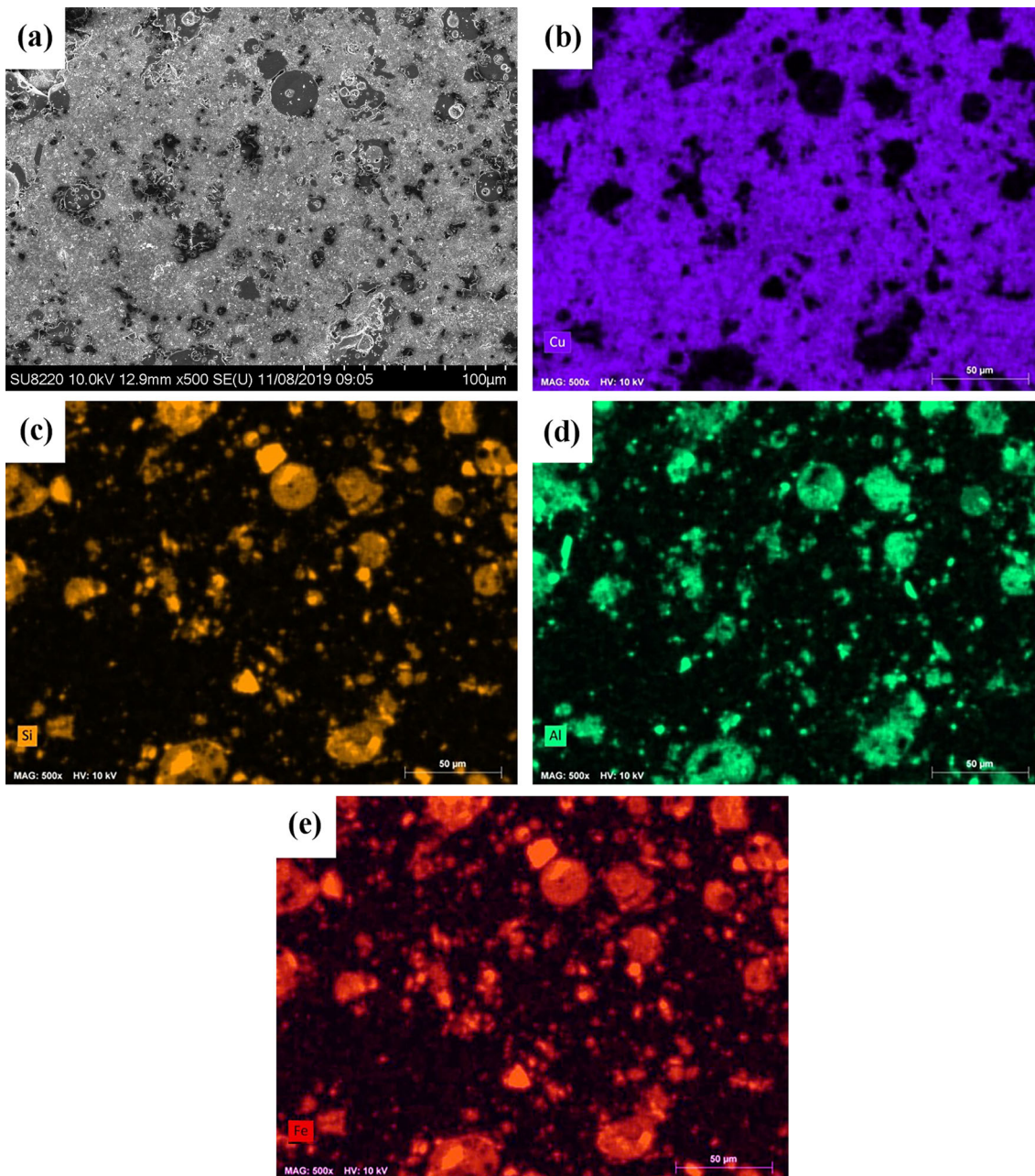


Fig. 7 (a) SEM micrograph of Cu/15 wt.% fly ash CMC and mapping of elements containing: (b) Cu, (c) Si, (d) Al, and (e) Fe

at higher content of fly ash particles. The grain refinement is beneficial to improve the performance of the composite.

3.4 Sliding Wear Behavior of Cu/Fly Ash Composites

The plots in Fig. 10 present the variation in wear rate and COF during sliding wear of Cu/fly ash CMCs as a function of fly particle content. The effective role of fly ash particle on wear rate and COF is well pronounced. The values of wear rate and COF were considerably reduced by the fly ash particles to that of the unreinforced copper matrix. The increase in fly ash particles content improved the wear resistance additionally. The wear rate was calculated to be $908 \times 10^{-5} \text{ mm}^3/\text{m}$ at 0 wt.% fly ash and $479 \times 10^{-5} \text{ mm}^3/\text{m}$ at 20 wt.% fly ash. The COF was calculated to be 0.55 at 0 wt.% fly ash and 0.35 at 20 wt.%

fly ash. The wear tests prove that fly ash reinforcement is favorable in enhancing the wear resistance of CMCs. The enhancement in wear behavior can be understood by the subsequent factors, which bring down the rate of material removal at the sliding interface. The reinforced fly ash particle is multiple times harder compared to unreinforced copper matrix. Reinforcing a hard ceramic particle imparts its hardness to the composite according to the rule of mixture (Ref 39). The resultant composite is harder than that of the initial unreinforced matrix. The improvement in hardness helps to resist the cutting action of the counterface asperities and reduce the material removal. This is stated in the famous expression derived by Archard (Ref 40). Since the reinforcement particle is much harder, uniform material removal across the contact surface does not occur in sliding a composite specimen. The

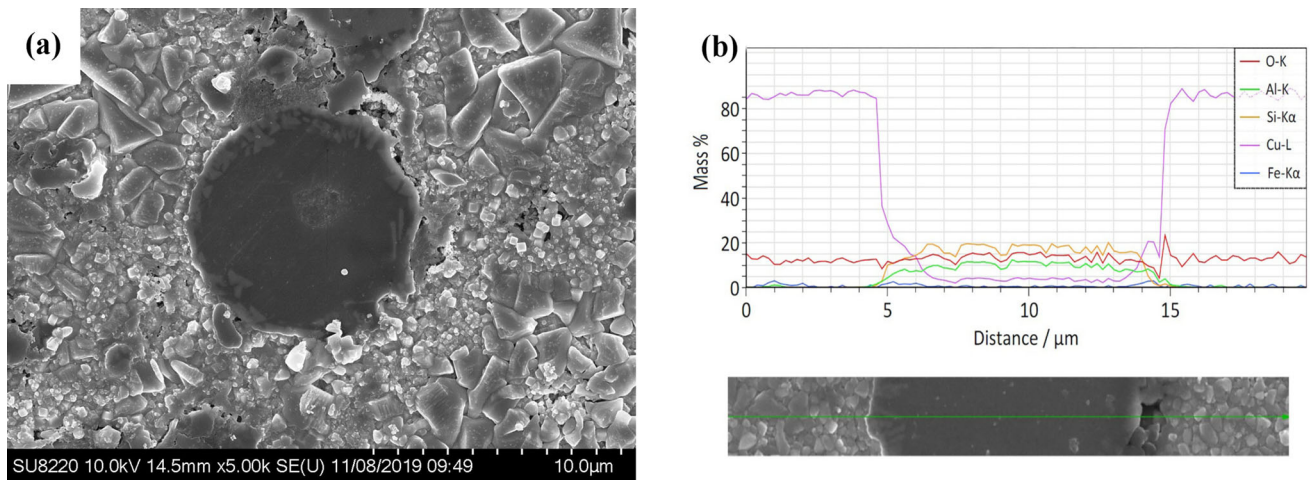


Fig. 8 (a) SEM micrograph of Cu/20 wt.% fly ash CMC and (b) line EDAX across a fly ash particle

soft copper material is initially removed with ease during sliding, which exposes a layer of protruding fly ash particles. The fly ash particles establish direct contact with the counterface. The applied normal load is supported by the fly particles because of good interfacial bonding. A proper bonding of fly ash particles with the copper matrix delays pulling the particle out in sliding wear. Further, direct contact reduces the cross-sectional area during sliding. The proper distribution of fly ash particles in the copper matrix helps to achieve a reduction in contact area when exposed. This reduced contact area is one of the reasons for bringing down the COF value. A reduction in COF is beneficial to slow down the material removal process during sliding wear. Further, the morphology of the fly particle plays a role during sliding. The spherical morphology avoids unnecessary building of stress at the interface with the copper matrix (Ref 41). Therefore, crack initiation to pull out or break the particle is retarded. The increase in fly ash particle content increases the hardness and reduces the contact area leading to further improvement in wear resistance. The plots in Fig. 10 are not perfectly linear because of the complexity of the wear process for a composite material dictated by the interaction of several factors. Figure 11 presents the changes in height loss and COF observed while carrying out the wear test. The frequency of changes in the plot of the copper matrix appears less compared to the fly ash-reinforced CMCs. The mode in which the material is removed, changes in the case of composites. The cycle of copper matrix removal, fly ash reinforcement pull out/detachment and fresh exposure of another layer of CMC to sliding action cause sharp variations in the plot of composites. The height loss suddenly increases or drops if a bunch of fly ash particles in the exposed layer detaches. This causes a corresponding variation in the COF plot. The disturbance in the plot is high at higher particle content because of the increased number of particles. Table 2 compares the COF values of the present work to similar composites reported in the literature. COF values are better than those few works (Ref 28, 30) and close to that of those reported by Balamurugan et al. (Ref 29). Although many carried out wear tests, COF values were not published. Table 2 shows that the prepared Cu/fly ash CMCs provide good wear performance.

Figure 12 presents the morphology of the worn surfaces after the wear test, recorded using SEM. The damage on the worn surface (Fig. 12) becomes lower at higher content of fly

ash particles. Figure 13 showcases the 3D profiles of selected worn surfaces recorded using a profilometer. The increase in fly ash content makes the surface profile (Fig. 13) smoother. The Ra value was computed as $4.91 \mu\text{m}$ at 0 wt.% fly ash and $1.01 \mu\text{m}$ at 20 wt.% fly ash. It confirms that the reinforcement of fly ash particles protected the subsurface from severe wear. The softer sliding surface of pure copper plasticizes easily during the course of sliding owing to the accumulation of frictional heat at the interface. The counterface cuts through the surface easily, and the material is removed in large proportions. Most of the worn surface is covered with large size pits (Fig. 12a). The surface is completely smashed off. The counterface asperities penetrated deep into the subsurface. The wear mode is recognized as microcutting. The 3D profile (Fig. 13a) displays many valleys and peaks, indicating severe wear. The increase in fly ash content reduces the size and the number of the pits. The incorporation of the fly ash particles strengthens the subsurface. The counterface encounters resistance to cutting action. The material removal rate is reduced. The worn surfaces at 15 wt.% (Fig. 12d) and 20 wt.% (Fig. 12e) do not show any presence of large-size pits. The surface is flat and covered with fine debris, which loosely adhere to the worn surface. The homogenous distribution of fly ash particles plays a crucial role in protecting the entire sub-surface. A poor particle distribution would result in localized spots of severe wear. A closer look at Fig. 12d and e reveals parallel line-like striations on the worn surface. This pattern is the result of abrasive wear behavior. The increase in fly ash content causes a shift in wear mode. The material removal is lower during abrasive wear. The 3D profile does not show deep valleys or taller peaks (Fig. 13c).

Figure 14 presents the morphology of the wear debris collected after the wear test observed using SEM. It is obvious that the reinforcement of the fly ash particles has an influence on the morphology and the size of debris produced throughout the sliding wear. The size of debris becomes smaller at higher particle content. The size of the debris exposes the nature of material removal and the mode of wear. The microcutting is stronger at lower volume content (≤ 10 wt.%). This is the reason for large size of debris in the micrographs (Fig. 15a-c). Nevertheless, some fine debris are accompanied with large size debris. This can be related to the initial collision of asperities of the counterface and the sliding specimen. The breakage of the

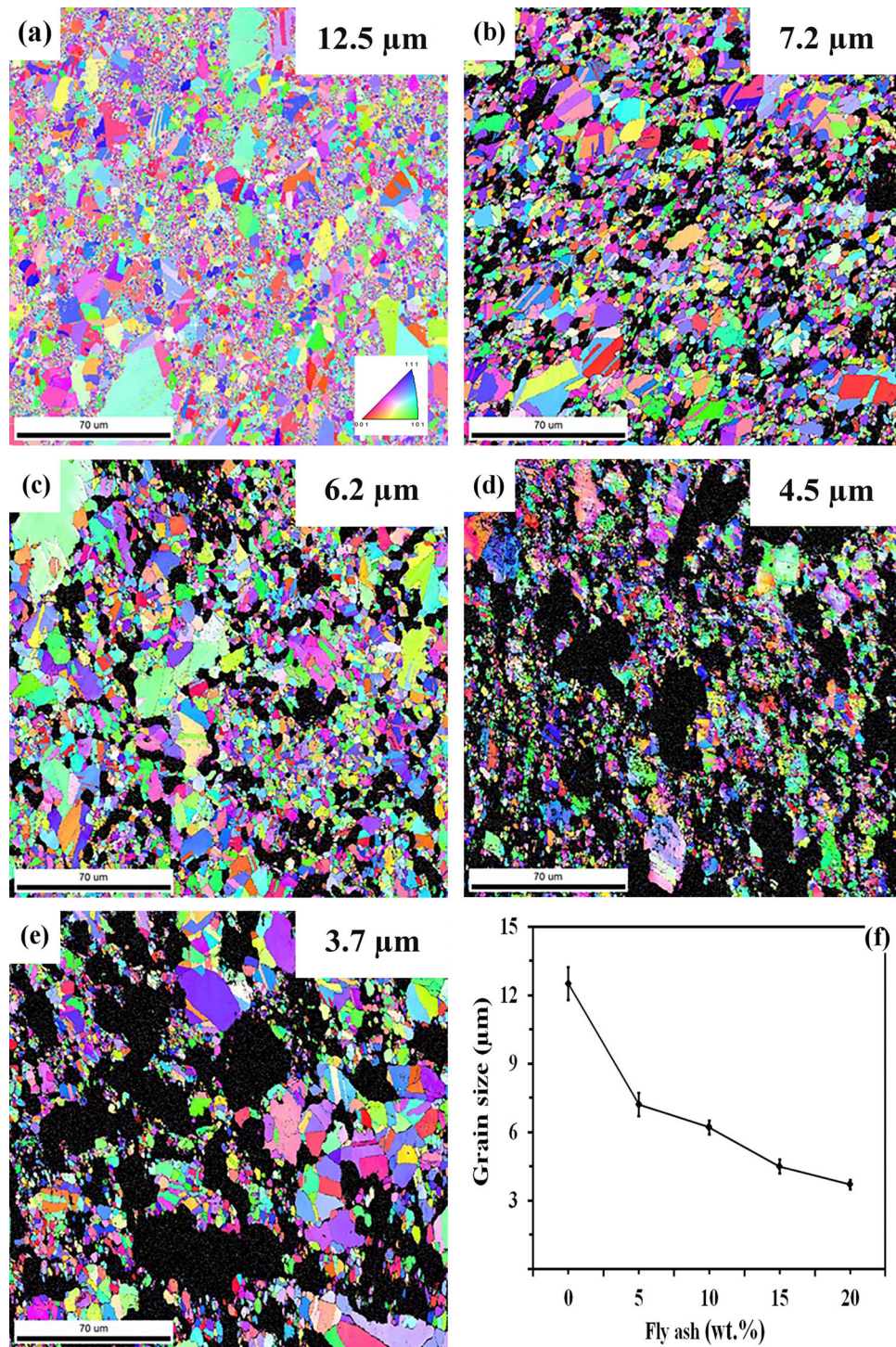


Fig. 9 EBSD (IPF + grain boundary) maps of Cu/fly ash CMCs containing fly ash particles: (a) 0 wt.%, (b) 5 wt.%, (c) 10 wt.%, (d) 15 wt.%, (e) 20 wt.%, and (f) effect of fly ash on grain size

asperities during the initial stages of sliding generates such smaller size debris. Most of the large-size debris is not seen at higher particle content (15 wt.% and 20 wt.%). This can be ascribed to two factors. The higher content provided enough strengthening so that the counterface was not able to cut deeply into the subsurface. Material is removed in smaller quantities. Secondly, the debris generated is thrown on the sliding path over the counterface. The rotation of the counterface brings that

debris into the sliding interface cyclically. They are ground repeatedly, similar to milling action in a ball mill. Therefore, the size is further reduced. That trapped debris cause a transition in the mode of wear into abrasive three-body wear. The material removal is decreased further, and the wear resistance is enhanced. Therefore, the wear debris is finer at higher fly ash particle content.

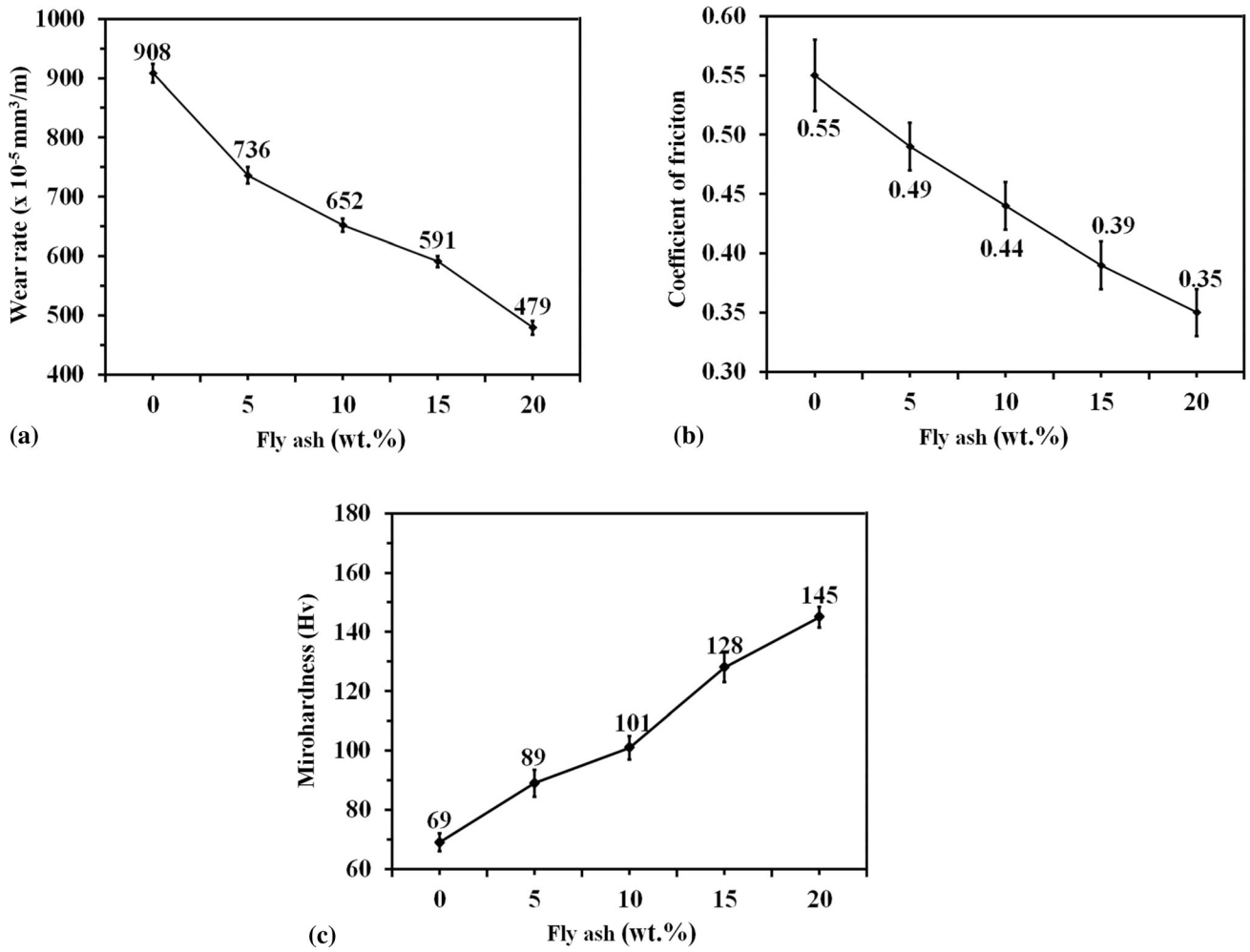


Fig. 10 Plots showing: (a) wear rate, (b) coefficient of friction, and (c) hardness of Cu/fly ash CMCs

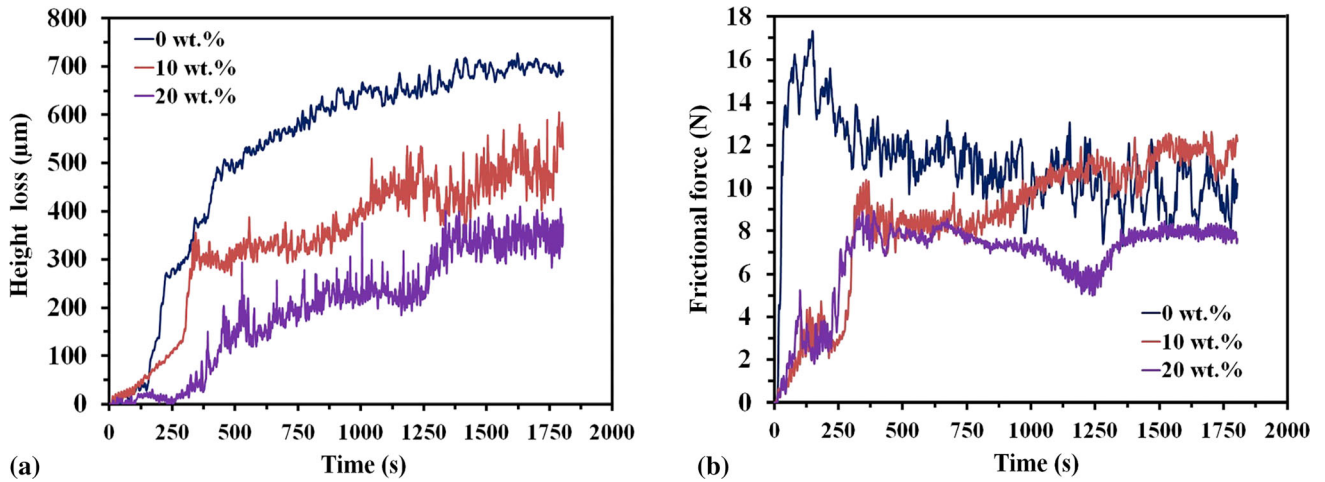


Fig. 11 Variation of: (a) height loss and (b) friction force of typical Cu/fly ash CMC samples during sliding wear

Table 2 Comparison of COF of Cu/fly ash CMCs with published works

References	Vol.%	COF
Present work	5	0.49
	10	0.44
	15	0.39
	20	0.35
Kasirajan et al. [28]	6	0.64
	12	0.68
Balamurugan et al. [29]	5	0.50
	10	0.45
Devaraju et al. [30]	5	0.61

3.5 Electrical Conductivity of Cu/Fly Ash Composites

Figure 15 shows the electrical conductivity of Cu/fly ash CMCs as a function of fly ash content. The electrical conductivity was measured as 80%IACS at 0 wt.% fly ash and 32%IACS at 20 wt.% fly ash. The incorporation of fly ash particles into the copper matrix brought down the values of electrical conductivity. The increased content of fly ash reduced the electrical conductivity further. The commonly used reinforcement particles usually reduce electrical conductivity (Ref 41). Copper possesses the highest electrical conductivity among the majority of metals. On the other hand, fly ash is a poor conductor of electricity. The dispersion of fly ash particles in the copper matrix acts as localized insulation sites. The resistance to conduct electricity increases. The interface

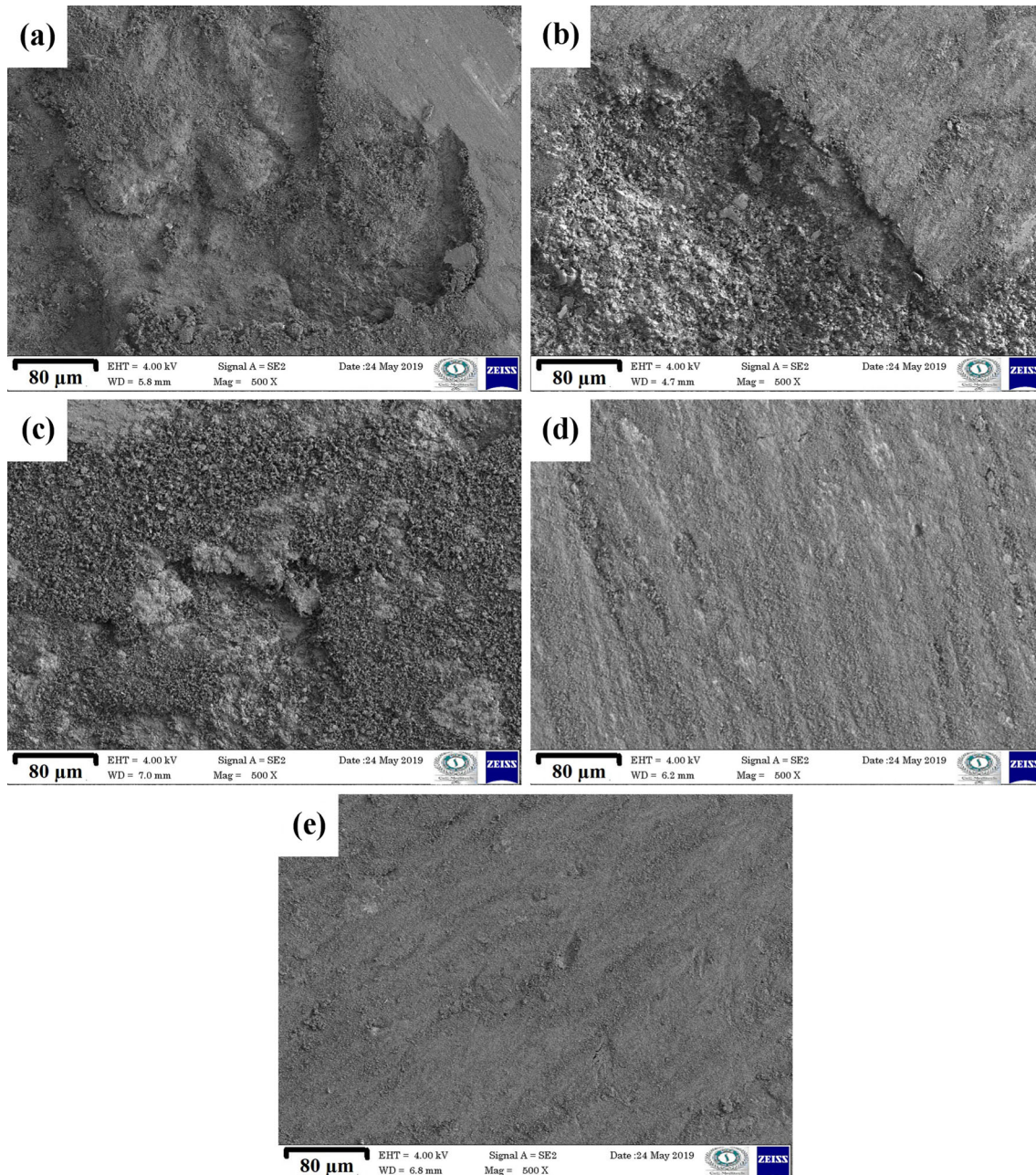


Fig. 12 SEM micrographs of worn surface of Cu/fly ash CMCs containing fly ash particles: (a) 0 wt.%, (b) 5 wt.%, (c) 10 wt.%, (d) 15 wt., and (e) 20 wt.%

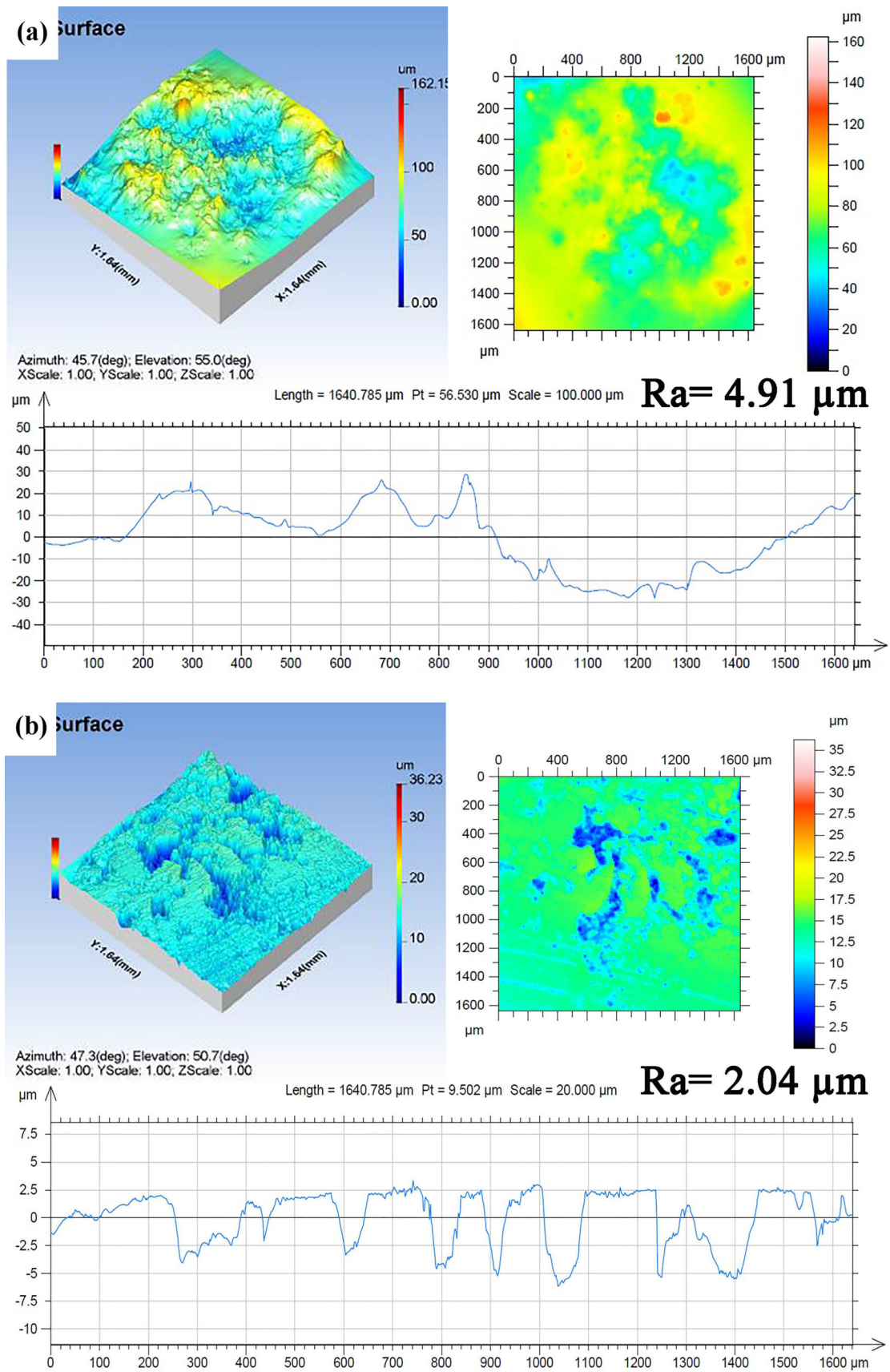


Fig. 13 Worn surface topography of Cu/fly ash CMCs containing fly ash particles: (a) 0 wt.%, (b) 10 wt.%, and (c) 20 wt.%

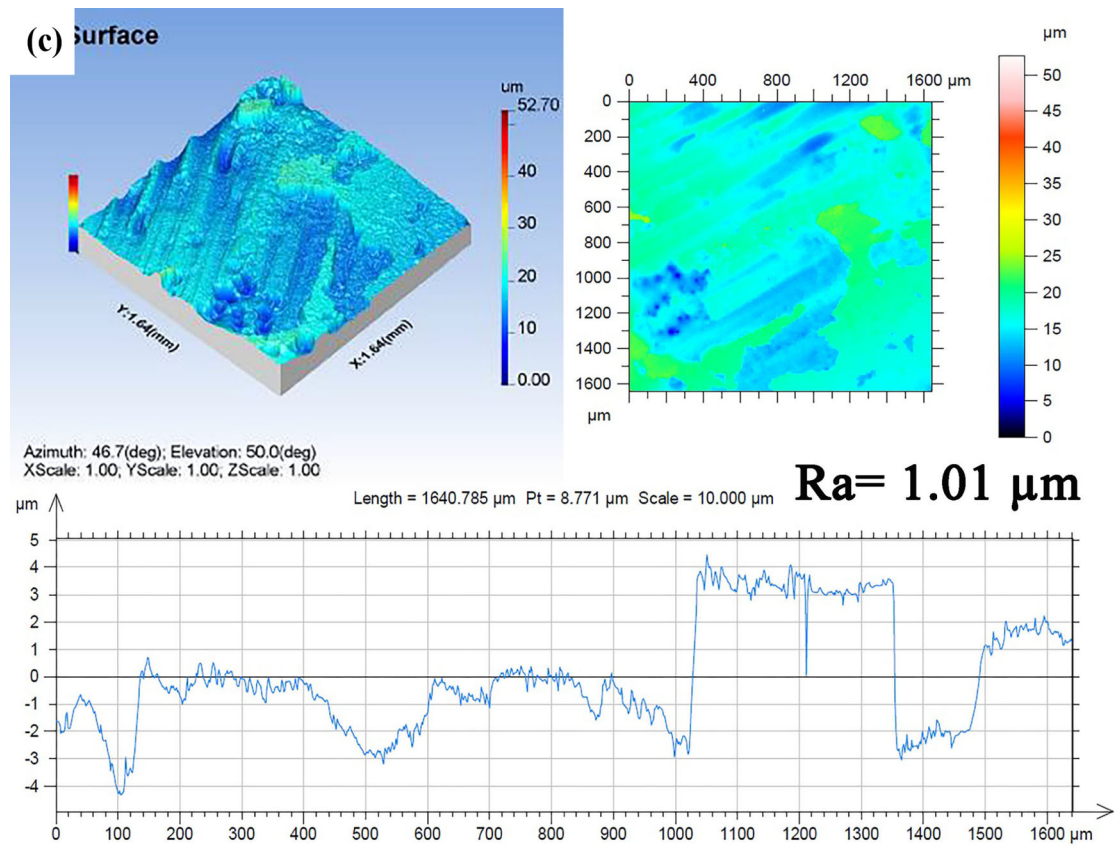


Fig. 13 continued

between copper and fly ash is a probable source to scatter the electron flow (Ref 28). More barriers are introduced along the path in which the electricity flows due to the grain refinement of the copper matrix. Not only grain refinement but porosity also acts as a barrier to the free flow of electrons. The aforementioned factors contribute to the reduction in the electrical conductivity of the fabricated CMCs.

4. Conclusions

- XRD plots did not show any formation of other oxides or interfacial reaction products. The protected atmosphere of the furnace avoided excessive oxidation.
- SEM micrographs demonstrated the proper distribution of fly ash particles in the composite. Few clusters were spotted at higher particle content. Large size pores or voids were not present.
- The density was estimated to be 8826 kg/m^3 at 0 wt.% fly ash and 7048 kg/m^3 at 20 wt.% fly ash. The porosity content was computed as 1.5% at 0 wt.% fly ash and 7.6% at 20 wt.% fly ash. The drop in density was ascribed to the lower density of fly ash particles, and its role in acting as a barrier to diffusion mechanism during sintering.
- EBSD images revealed that the increase in fly ash particle content caused a reduction in grain structure. Line EDAX confirmed an excellent interfacial bonding between copper and fly particles without reaction products or pores.
- The wear rate was calculated to be $908 \times 10^{-5} \text{ mm}^3/\text{m}$ at 0 wt.% fly ash and $479 \times 10^{-5} \text{ mm}^3/\text{m}$ at 20 wt.% fly ash. The COF was calculated as 0.55 at 0 wt.% fly ash and 0.35 at 20 wt.% fly ash. The improved wear behavior was related to the higher hardness and proper distribution

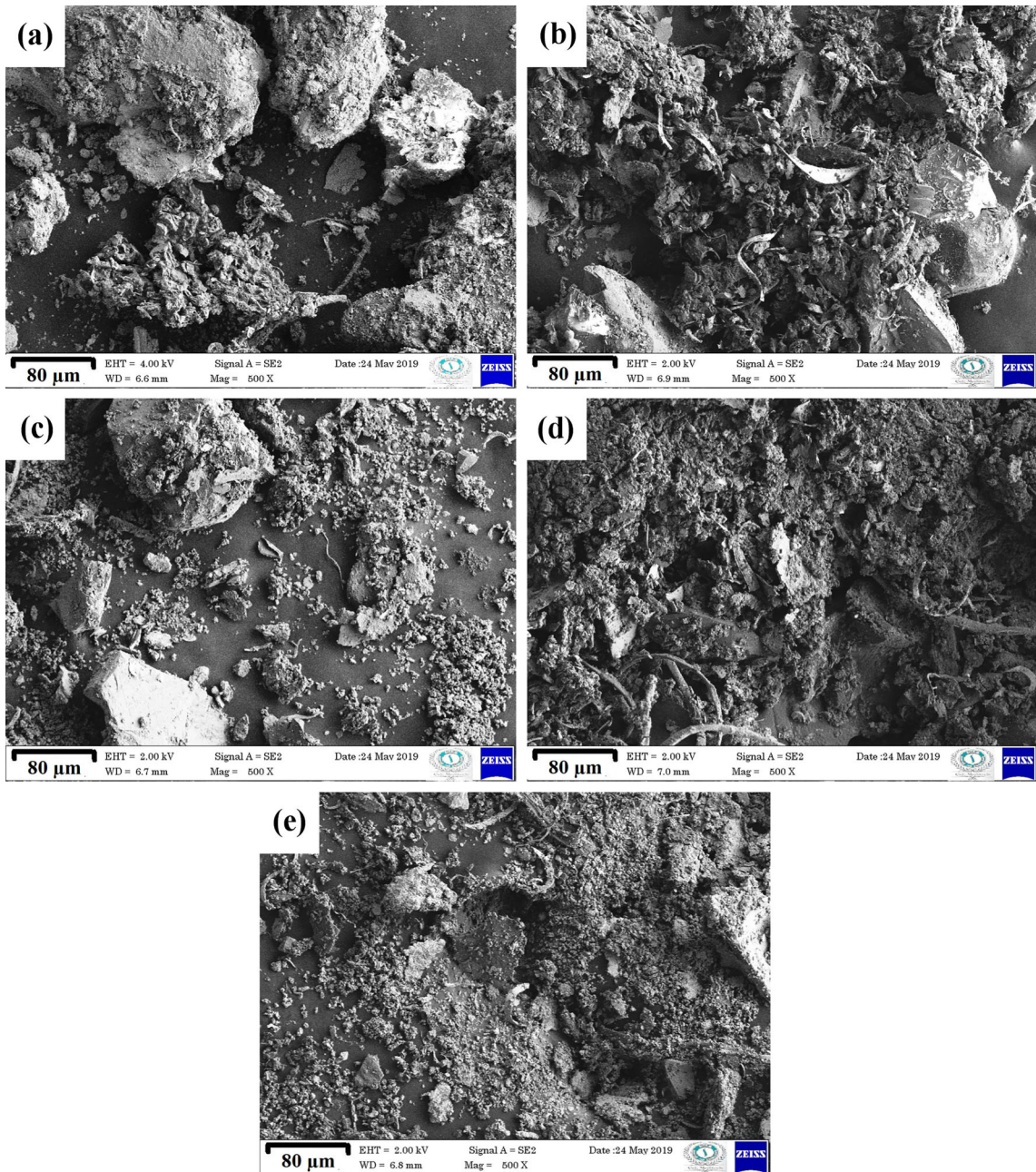


Fig. 14 SEM micrographs of wear debris of Cu/fly ash CMCs containing fly ash particles: (a) 0 wt.%, (b) 5 wt.%, (c) 10 wt.%, (d) 15 wt.%, and (e) 20 wt.%

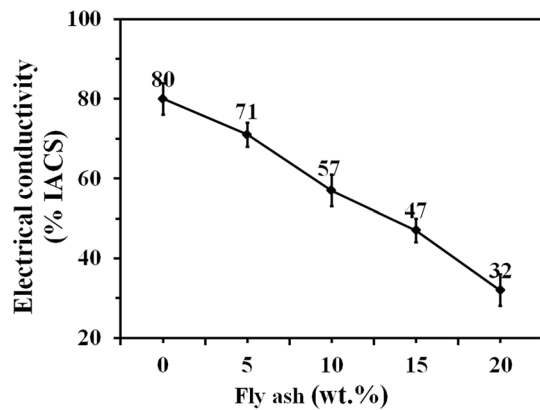


Fig. 15 Effect of fly ash on electrical conductivity of Cu/fly ash CMCs

of the fly ash particles, excellent interfacial bonding and reduction in effective contact area during sliding.

- The reinforcement of the fly ash particles diminished the electrical conductivity of the copper composite. The electrical conductivity was measured to be 80% IACS at 0 wt.% fly ash and 32% IACS at 20 wt.% fly ash.

Acknowledgments

The authors are grateful to Tuticorin Thermal Power Station at Tuticorin, V V College of Engineering at Tisaiyanvilai, Speed Spark EDM at Coimbatore, VV Titanium Pigments at Thoothukudi, Tii Techno Testing Services Pvt. Ltd at Chennai, The South India Textile Research Association (SITRA) at Coimbatore, OIM and Texture Lab at Indian Institute of Technology Bombay, Centre for Research in Metallurgy at Karunya University and Centre for NEMS and Nanophotonics at Indian Institute of Technology Madras for providing the facilities and materials to carry out this investigation.

Data availability statement

The raw/processed data required to reproduce these findings cannot be shared at this time due to legal or ethical reasons. The raw/processed data required to reproduce these findings cannot be shared at this time due to technical or time limitations.

References

1. Y. Mazaheri, M. Bahiraei, M.M. Jalilvand, S. Ghasemi, and A. Heidarpour, Improving Mechanical and Tribological Performances of Pure Copper Matrix Surface Composites Reinforced by Ti_2AlC MAX Phase and MoS_2 Nanoparticles, *Mater. Chem. Phys.*, 2021, **270**, p 124790
2. E.Z. Xu, J.X. Huang, Y.C. Li, Z.F. Zhu, M. Cheng, D.T. Li, H.H. Zhong, J.W. Liu, and Y. Jiang, Graphite Cluster/Copper-Based Powder Metallurgy Composite for Pantograph Slider with Well-Behaved Mechanical and Wear Performance, *Powder Technol.*, 2019, **344**, p 551–560
3. T.J. Li, Y.Q. Wang, M. Yang, H.L. Hou, and S.J. Wu, High Strength and Conductivity Copper Matrix Composites Reinforced by In-Situ Graphene Through Severe Plastic Deformation Processes, *J. Alloys Compd.*, 2021, **851**, p 156703
4. Y. Bian and J.J. Ni, Microstructure Evolution and Properties of In Situ Micro/Nanoscale Mo_2C Reinforced Copper Composite Synthesized by Hot-Pressing Consolidation of Mechanical Alloying Powders, *J. Mater. Eng. Perform.*, 2022, **31**, p 4604–4610
5. A. Jamwal, P.P. Seth, D. Kumar, R. Agrawal, K.K. Sadasivuni, and P. Gupta, Microstructural, Tribological and Compression Behaviour of Copper Matrix Reinforced with Graphite-SiC Hybrid Composites, *Mater. Chem. Phys.*, 2020, **251**, p 123090
6. L.H. Fu, M. Zhou, Y. Gao, Y.Z. Zhang, S.M. Du, Y. Zhang, Y. Yue, and Y.S. Mao, Effect of Interface Oxidation Treatment on the Interfacial Reactions and Wear Properties of Co-continuous SiC_3D/Cu Composites, *Ceram. Int.*, 2022, **48**, p 7784–7795
7. G. Nageswaran, S. Natarajan, and K.R. Ramkumar, Synthesis, Structural Characterization, Mechanical and Wear Behavior of Cu-TiO₂-Gr Hybrid Composite Through Stir Casting Technique, *J. Alloys Compd.*, 2018, **768**, p 733–741
8. J. Jabinth and N. Selvakumar, Experimental Investigation of Mechanical and Wear Behaviour of Cu-V₂O₅-Gr(L) Reinforced Composites, *Mater. Lett.*, 2022, **306**, p 130925
9. M. Ebrahimi and M.A. Par, Twenty-Year Uninterrupted Endeavor of Friction Stir Processing by Focusing on Copper and Its Alloys, *J. Alloys Compd.*, 2019, **781**, p 1074–1090
10. H. Kumar, R. Prasad, and P. Kumar, Effect of Multi-groove Reinforcement Strategy on Cu/SiC Surface Composite Fabricated by Friction Stir Processing, *Mater. Chem. Phys.*, 2020, **256**, p 123720
11. T. Thankachan, K. SooryaPrakash, and V. Kavimani, Investigations on the Effect of Friction Stir Processing on Cu-BN Surface Composites, *Mater. Manuf. Process.*, 2018, **33**, p 299–307
12. A. Heidarzadeh, H. Pouraliakbar, S. Mahdavi, and M.R. Jandaghi, Ceramic Nanoparticles Addition in Pure Copper Plate: FSP Approach, Microstructure Evolution and Texture Study Using EBSD, *Ceram. Int.*, 2018, **44**, p 3128–3133
13. N. Vijay Ponraj, A. Azhagurajan, S.C. Vettivel, X. SahayaShajan, P.Y. Nabhiraj, and M. Sivapragash, Graphene Nanosheet as Reinforcement Agent in Copper Matrix Composite by Using Powder Metallurgy Method, *Surf. Interfaces*, 2017, **6**, p 190–196
14. E. Sap, Microstructural and Mechanical Properties of Cu-Based Co-Mo-Reinforced Composites Produced by the Powder Metallurgy Method, *J. Mater. Eng. Perform.*, 2020, **29**, p 8461–8472
15. J.P. Huang, M. Tayyebi, and A.H. Assari, Effect of SiC Particle Size and Severe Deformation on Mechanical Properties and Thermal Conductivity of Cu/Al/Ni/SiC Composite Fabricated by ARB Process, *J. Manuf. Process.*, 2021, **68**, p 57–68
16. X.Y. Zhou, Z. Hu, and D.Q. Yi, Enhancing the Oxidation Resistance and Electrical Conductivity of Alumina Reinforced Copper-Based Composites via Introducing Ag and Annealing Treatment, *J. Alloys Compd.*, 2019, **787**, p 786–793
17. A.M. Lopez, C.A.L. Patino, E.A.A. Reyes, E.B. Becerril, and G.R. Ortiz, Effect of Graphite Addition on Wear Behaviour of Hybrid Cu/TiC-Gr Infiltrated Composites, *Wear*, 2021, **484–485**, p 203793
18. P.K. Prajapati and D. Chaira, Fabrication and Characterization of Cu-B₄C Metal Matrix Composite by Powder Metallurgy: Effect of B₄C on Microstructure, Mechanical Properties and Electrical Conductivity, *Trans. Indian Inst. Met.*, 2019, **72**, p 673–684
19. S.H. Pan, T.Q. Zheng, G.C. Yao, Y.T. Chi, I.D. Rosa, and X.C. Li, High-Strength and High-Conductivity In Situ Cu-TiB₂ Nanocomposites, *Mater. Sci. Eng. A*, 2022, **831**, p 141952
20. I. Dinaharan and E.T. Akinlabi, Low Cost Metal Matrix Composites Based on Aluminum, Magnesium and Copper Reinforced with Fly Ash Prepared Using Friction Stir Processing, *Compos. Commun.*, 2018, **9**, p 22–26
21. A. Bahrami, N. Soltani, M.I. Pech-Canul, and C.A. Gutiérrez, Development of Metal-Matrix Composites from Industrial/Agricultural Waste Materials and Their Derivatives, *Crit. Rev. Environ. Sci. Technol.*, 2016, **46**, p 143–208
22. A.K. Kasar, N. Gupta, P.K. Rohatgi, and P.L. Menezes, A Brief Review of Fly Ash as Reinforcement for Composites with Improved Mechanical and Tribological Properties, *JOM*, 2020, **72**, p 2340–2351
23. C. Lanzerstorfer, Fly Ash from Coal Combustion: Dependence of the Concentration of Various elements on the Particle Size, *Fuel*, 2018, **228**, p 263–271
24. M. Ahmaruzzaman, A Review on the Utilization of Fly Ash, *Prog. Energy Combust. Sci.*, 2010, **36**, p 327–363

25. N.V. Sai, M. Komaraiah, and A.V.S.R. Raju, Preparation and Properties of Sintered Copper–Tin Composites Containing Copper Coated or Uncoated Fly Ash, *Mater. Manuf. Process.*, 2008, **23**, p 651–657
26. P.Y. Chew, S. Zahi, A.H. You, P.S. Lim, and M.C. Ng, Preparation of Cu and Fly Ash Composite by Powder Metallurgy Technique, *AIP Conf. Proc.*, 2011, **1328**, p 208–210
27. P. Balamurugan and M. Uthayakumar, Influence of Process Parameters on Cu–Fly Ash Composite by Powder Metallurgy Technique, *Mater. Manuf. Process.*, 2015, **30**, p 313–319
28. S.T. Kasirajan, A.N. Balaji, P. Narayanasamy, and S.C. Vettivel, Microstructural, Electrical, Thermal and Tribological Studies of Copper–Fly Ash Composites Through Powder Metallurgy, *Bull. Acad. Pol. Sci.*, 2018, **66**, p 935–940
29. P. Balamurugan, M. Uthayakumar, and M.N. Wójcik, Wear Studies of Copper–Fly Ash Composite Under Dry Sliding Conditions, *Mater. Res. Express*, 2019, **6**, p 1065d5
30. A. Devaraju, P. Sivasamy, R. Gopi, and A. Muthiah, Studies on Wear Behaviour of Silicon Carbide and Fly Ash Reinforcedcopper Based Metal Matrix Composites, *Mater. Today Proc.*, 2021, **39**, p 888–891
31. R. Rajesh, B. Shankar, J. Hari Krishnan, A. Ritwik, A. Hari Krishna, Q. Usman, and R. HariSankar, Study on Conventional and Microwave Assisted Sintering of Cu–FA COMPOSITES, *Mater. Today Proc.*, 2021, **39**, p 1677–1681
32. I. Dinaharan and T. Albert, Effect of Reinforcement Type on Microstructural Evolution and Wear Performance of Copper Matrix Composites via Powder Metallurgy, *Mater. Today Commun.*, 2023, **34**, p 105250
33. C. Suryanarayana and N. Al-Aqeeli, Mechanically Alloyed Nanocomposites, *Prog. Mater. Sci.*, 2013, **58**, p 383–502
34. S.C. Vettivel, N. Selvakumar, and N. Leema, Experimental and Prediction of Sintered Cu–W Composite by Using Artificial Neural Networks, *Mater. Des.*, 2013, **45**, p 323–335
35. G.C. Efe, T. Yener, I. Altinsoy, M. Ipek, S. Zeytin, and C. Bindal, The Effect of Sintering Temperature on Some Properties of Cu–SiC Composite, *J. Alloys Compd.*, 2011, **509**, p 6036–6042
36. A. Jamwal, P. Mittal, R. Agrawal, S. Gupta, D. Kumar, K.K. Sadasivuni, and P. Gupta, Towards Sustainable Copper Matrix Composites: Manufacturing Routes with Structural, Mechanical, Electrical and Corrosion Behaviour, *J. Compos. Mater.*, 2020, **54**, p 2635–2649
37. G.C. Efe, M. Ipek, S. Zeytin, and C. Bindal, An Investigation of the Effect of SiC Particle Size on Cu–SiC Composites, *Compos. Part B*, 2012, **43**, p 1813–1822
38. R. Mitra and Y.R. Mahajan, Interfaces in Discontinuously Reinforced Metal Matrix Composites: An Overview, *Bull. Mater. Sci.*, 1995, **18**, p 405–434
39. H.S. Kim, On the Rule of Mixtures for the Hardness of Particle Reinforced Composites, *Mater. Sci. Eng. A*, 2000, **289**, p 30–33
40. J.F. Archard, Contact and Rubbing of Flat Surfaces, *J. Appl. Phys.*, 1953, **24**, p 981–988
41. I. Solodkyi, O. Bezdorozhev, and P. Loboda, High Electrical Conductive Copper Matrix Composites Reinforced with LaB₆-TiB₂ Eutectic Particles, *Vacuum*, 2020, **177**, p 109407

Publisher's Note Springer Nature remains neutral with regard to jurisdictional claims in published maps and institutional affiliations.

Springer Nature or its licensor (e.g. a society or other partner) holds exclusive rights to this article under a publishing agreement with the author(s) or other rightsholder(s); author self-archiving of the accepted manuscript version of this article is solely governed by the terms of such publishing agreement and applicable law.